Supplementary Information (SI) for Nanoscale.

Supplementary Material

Immobilization of Horseradish Peroxidase on UIO-66-NH_2 for Colorimetric and Fluorometric Sensing of Nitrite

Zuyao Fu [a], Lingfeng Yang [a], Zhaoyang Ding [a,b,c *], Jing Xie [a,b *]

a College of Food Science and Technology, Shanghai Ocean University, Shanghai 201306, China

b Shanghai Engineering Research Center of Aquatic-Product Processing & Preservation, Shanghai 201306, China

c Marine Biomedical Science and Technology Innovation Platform of Lin-gang Special Area, Shanghai 201306, China

* Corresponding authors. E-mail addresses: zyding@shou.edu.cn (Z. Ding); jxie@shou.edu.cn (J. Xie).

Characterizations

The morphology of the materials was observed using a Talos F200X transmission electron microscope (TEM) and an SU5000 scanning electron microscope (SEM). X-ray diffraction (XRD) measurements were obtained using an Ultima IV diffractometer. Fourier transform infrared spectroscopy spectra (FTIR) were recorded with a Nicolet iS5 spectrometer. Particle size and zeta potential were measured using a Zetasizer Pro Nanoparticle Size and Zeta Potential Analyzer. X-ray photoelectron spectroscopy (XPS) analysis was performed with an EscaLab 250Xi spectrometer. CLSM images were taken on Leica SP5. Ultraviolet-visible absorption spectra were acquired using a U-3900 spectrophotometer. Fluorescence signals were recorded using an F-7000 spectrophotometer.

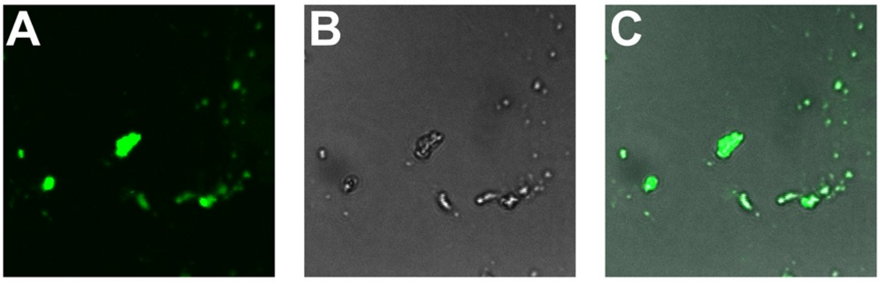

Figure S1. CLSM images of (A) fluorescent, (B) optical, and (C) overlap of optical and fluorescent images of HRP@UiO-66-NH_2.

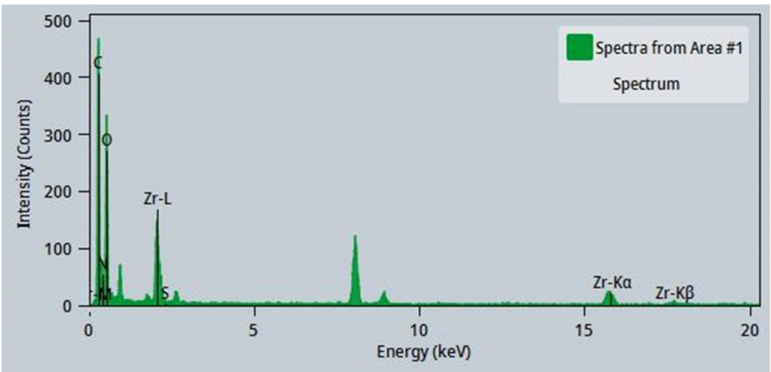

Figure S2. EDS pattern of UiO-66-NH_2.

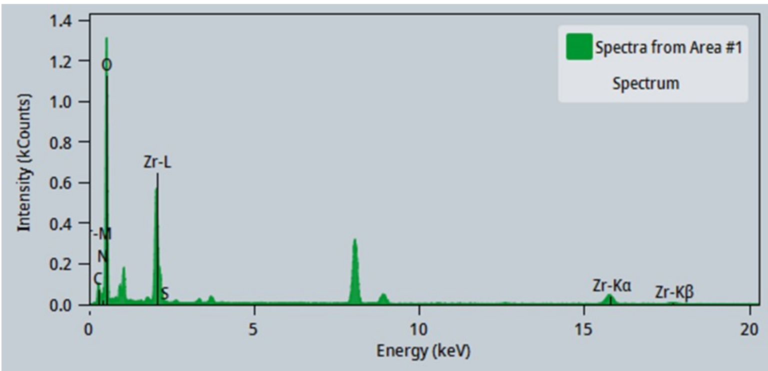

Figure S3. EDS pattern of HRP@UiO-66-NH_2

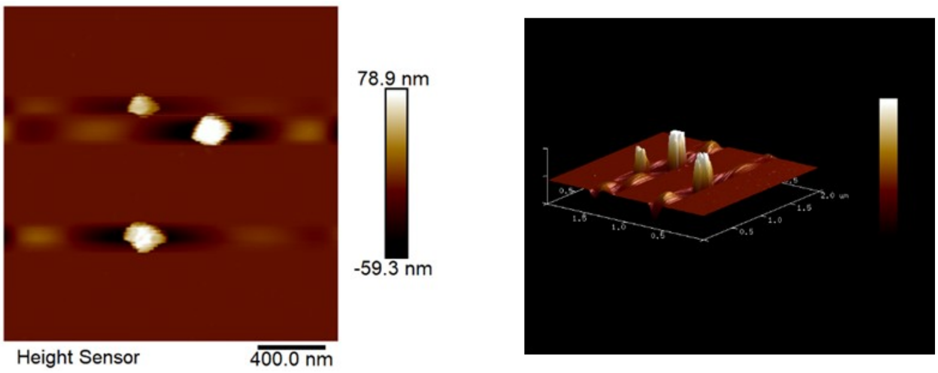

Figure S4. AFM pattern of UiO-66-NH_2.

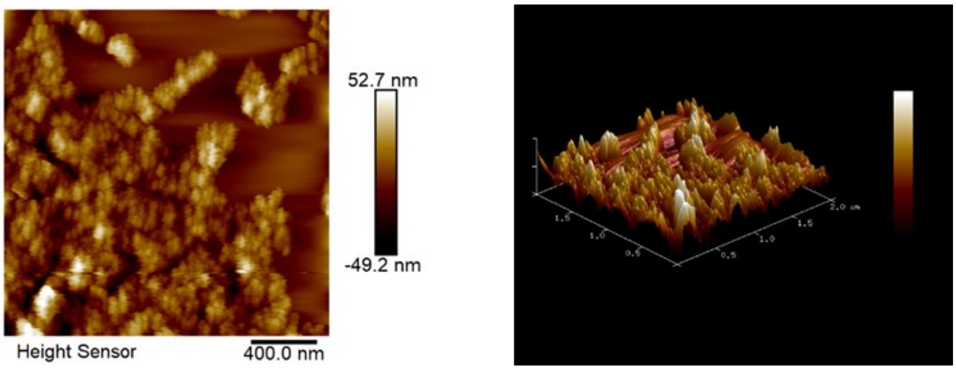

Figure S5. AFM pattern of UiO-66-NH_2.

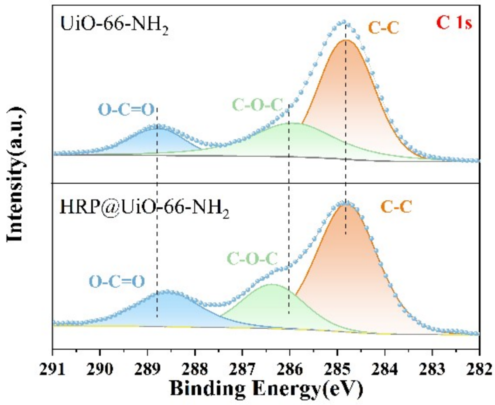

Figure S6. C 1s high resolution XPS spectra of UiO-66-NH_2 (top) and HRP@UiO-66-NH_2 (below).

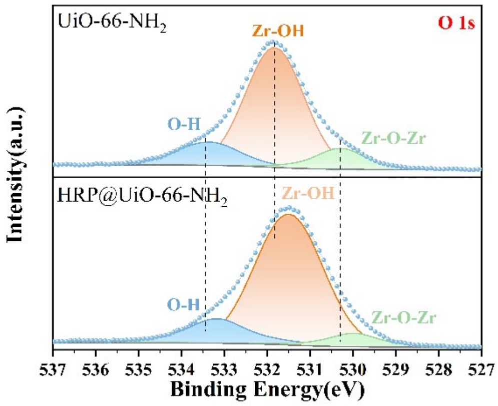

Figure S7. O 1s high resolution XPS spectra of UiO-66-NH_2 (top) and HRP@UiO-66-NH_2 (below).

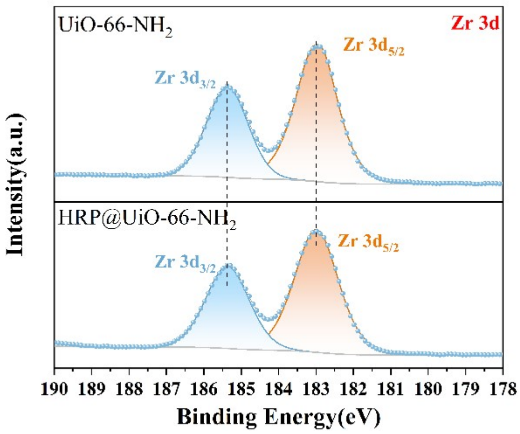

Figure S8. Zr 3d high resolution XPS spectra of UiO-66-NH_2 (top) and HRP@UiO-66-NH_2 (below).

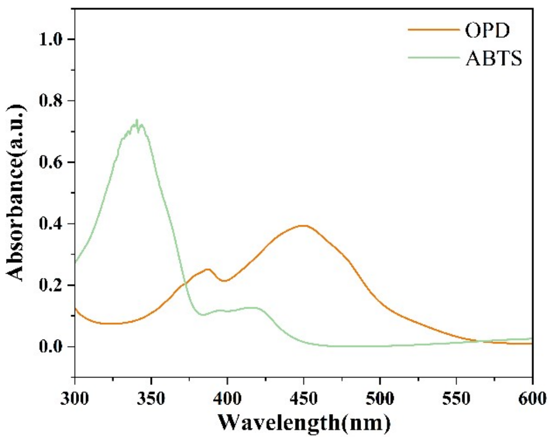

Figure S9. UV−vis absorption patterns of HRP@UiO-66-NH_2 + OPD + H_2O_2 and HRP@UiO-66-NH_2 + ABTS + H_2O_2.

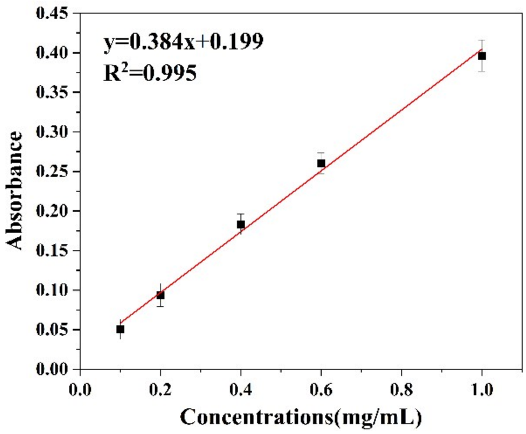

Figure S10. The standard curve of absorbance and BSA concentration.

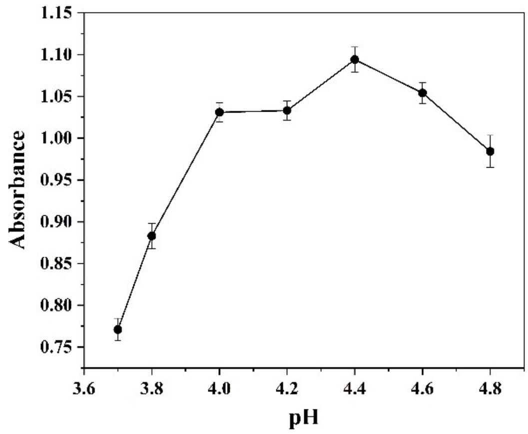

Figure S11. Effect of buffer pH on the absorbance of HRP@UiO-66-NH_2 + TMB + H_2O_2.

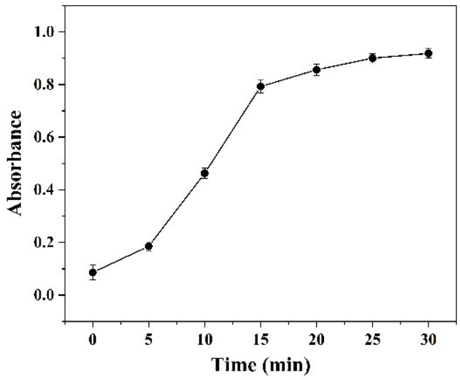

Figure S12. The absorbance of HRP@UiO-66-NH_2 + TMB + H_2O_2 at different time.

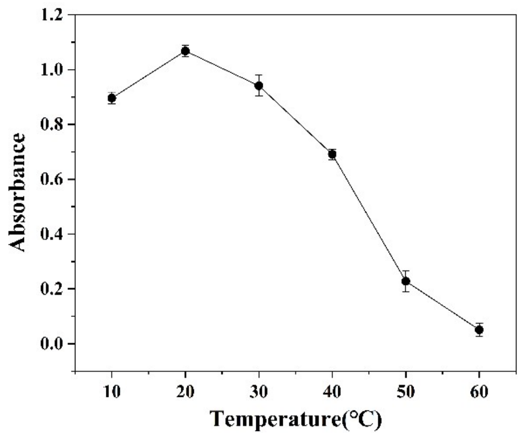

Figure S13. Effect of temperature on the absorbance of HRP@UiO-66-NH_2 + TMB + H_2O_2.

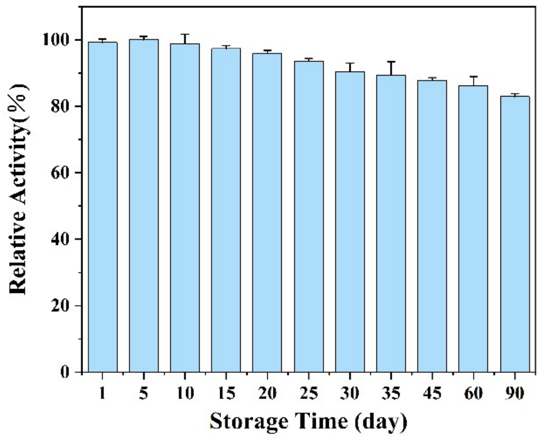

Figure S14. Oxidase-mimetic activity stability of HRP@UiO-66-NH_2 during storage

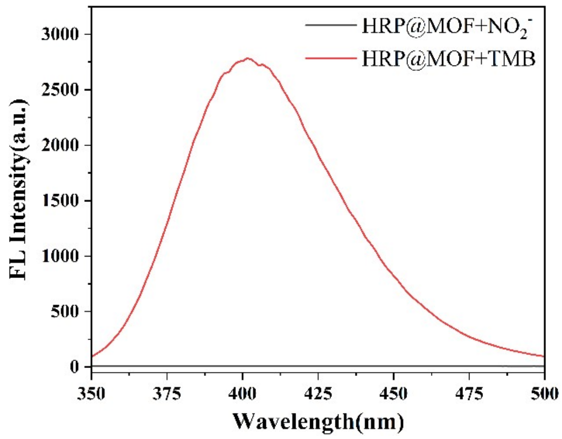

Figure S15. Fluorescence spectra of HRP@UiO-66-NH_2 in the presence and absence of NO_2^-.

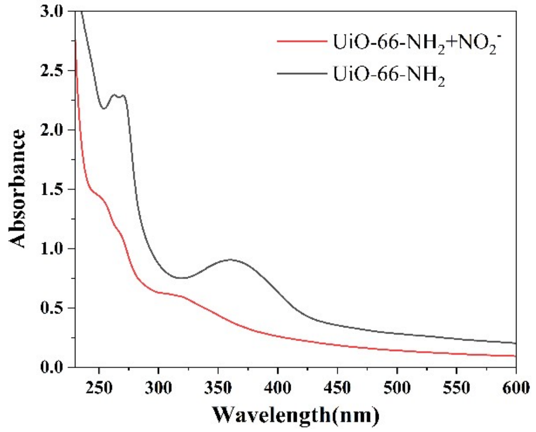

Figure S16. UV−vis absorption spectra of HRP@UiO-66-NH_2 in the presence and absence of NO_2^-.

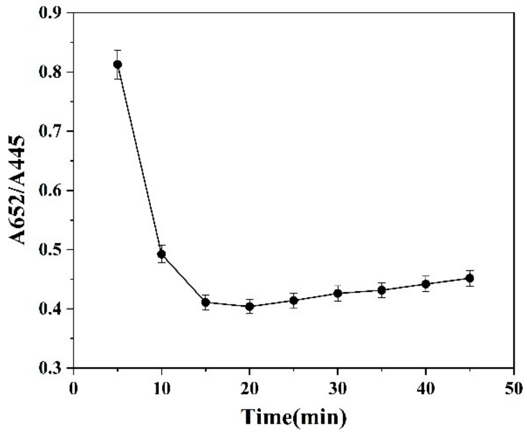

Figure S17. Effect of time on the colorimetric signal A652/A445 along with the diazotization time of TMB^+ and NO_2^-.

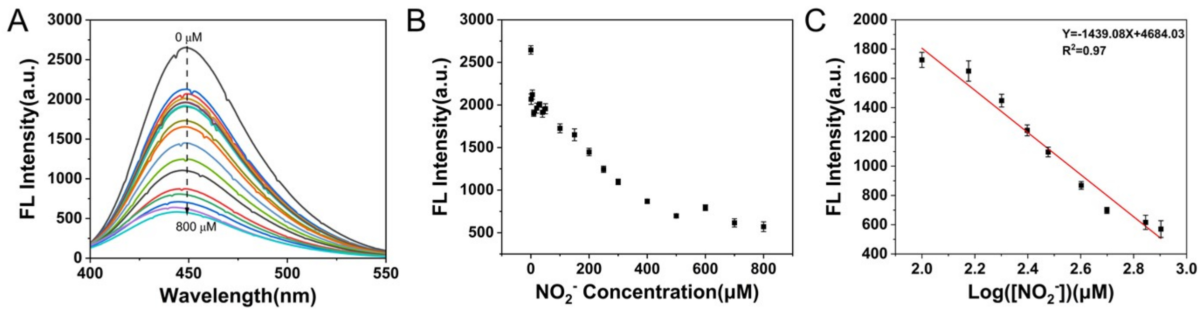

Figure S18. The response of UiO-66-NH_2 towarded nitrite.

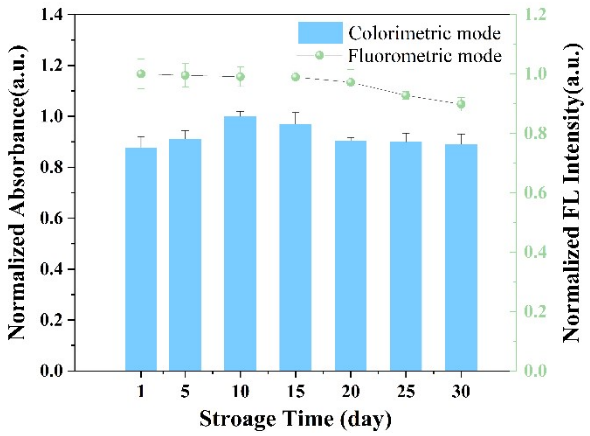

Figure S19. The stability of colorimetric/fluorometric dual-mode sensors.

Table S1The calculated catalytic kinetic parameters for free enzymes and HRP@UiO-66-NH_2

substrate	enzyme probe	K_m (mM)	V_{max} (M s^{-1})	K_{cat} (s^{-1})
TMB	HRP@UiO-66-NH_2	0.23	15.36×10^{-8}	6.14×10^3
	Free HRP	0.434	10.00×10^{-8}	4.00×10^3
H_2O_2	HRP@UiO-66-NH_2	1.00	2.36×10^{-8}	0.94×10^3
	Free HRP	3.70	8.71×10^{-8}	3.48×10^3

Table S2 Comparison of the reusability presented in this work with that reported previously.

Enzyme@(material)	Reusability	Residual activity	Ref
HRP@UiO-66-NH_2	10	75.76%	This work
HRP@(amidoximated acrylic polymer)	10	45.0%	[1]
HRP@(functionalized reduced graphene oxide)	10	70%	[2]
HRP@(electrospun magnetic nanofibers)	5	52%	[3]
HRP@(functionalized reduced graphene oxide-SiO_2)	10	70%	[4]
HRP@(cationic microporous starch)	10	66%	[5]
HRP@CN/$Cu_3(PO_4)_2$	5	83.6%	[6]
HRP@(PDA/expanded polystyrene foam)	15	60%	[7]

Table S3 Performance comparison of our colorimetric/fluorometric method with previously reported approaches for nitrite detection

Sensor Material	Year	Detection mode	Detecting range	Detection limit	Ref.
UiO-66-NH_2	2020	Fluorometric	0–10 mM	77 µM	[8]
UiO-66-NH_2-Cit	2020	Fluorometric	0–800 µM	–	[9]
Tb-MOF	2021	Fluorometric	4–200 µM	1.25 µM	[10]
Eu^{3+}@UiO-66-$(COOH)_2$	2021	Fluorometric	0–60 µM	0.69 µM	[11]
MnFeO	2021	Colorimetric	3.3~133.3.3µM	0.2 µM	[12]
MnCDs	2022	Colorimetric	2−150 µM,	0.16 µM	[13]

		Fluorometric	2 to 150 μM	1.07 μM	
CeO_2	2023	Colorimetric	2−100 μM	0.29 μM	14
Ru@UiO-66-NH_2	2024	Fluorometric	10.0 - 15.0 μM	0.3 μM	15
P–N–C nonmetal nanozymes	2024	Electrochemical	1–800 μM	0.21 μM	16
		Colorimetric	1 to 700 μM	0.24 μM	

Table S4 Detection results by our colorimetric/ fluorometric sensing platform of nitrite in real samples.

Detection mode	**Sample**	**Spiked (μM)**	**Detected (μM)**	**RSD (%, n=3)**	**Recovery (%)**
colorimetric	lake water	0	0.20	0.13	NA
		50	50.68	1.86	101.96
		100	89.31	0.92	89.11
	sausages	0	8.32	2.36	NA
		50	58.61	1.83	100.58
		100	107.93	4.61	99.61
	pickled fish	0	10.36	0.82	NA
		50	55.60	0.37	90.48
		100	105.75	1.64	95.39
	pickle brine	0	1.92	0.38	NA
		50	52.37	4.93	100.9
		100	101.49	1.73	99.57
Fluorometric	lake water	0	0.22	2.37	NA
		50	51.36	2.66	102.28
		100	103.84	1.87	103.62
	sausages	0	8.57	2.47	NA
		50	53.28	0.63	89.24
		100	109.83	1.79	101.26
	pickled fish	0	10.52	1.21	NA
		50	60.88	3.07	100.72
		100	104.39	0.93	93.87
	pickle brine	0	2.81	4.71	NA
		50	49.29	0.89	92.96
		100	103.82	5.32	101.01

NA = not applicable

Reference

1 S. A. Mohamed, S. S. Al-Ghamdi and R. M. El-Shishtawy, *Int J Biol Macromol*, 2016, **91**, 663–670.

2 M. Besharati Vineh, A. A. Saboury, A. A. Poostchi, A. M. Rashidi and K. Parivar, *Int J Biol Macromol*, 2018, **106**, 1314–1322.

3 J. Li, X. Chen, D. Xu and K. Pan, *Ecotoxicol Environ Saf*, 2019, **170**, 716–721.

4 M. B. Vineh, A. A. Saboury, A. A. Poostchi and A. Ghasemi, *Int J Biol Macromol*, 2020, **164**, 4403–4414.

5 M. E. El-Naggar, A. M. Abdel-Aty, A. R. Wassel, N. M. Elaraby and S. A. Mohamed, *Int J Biol Macromol*, 2021, **181**, 734–742.

6 J. Wu, X. Ma, C. Li, X. Zhou, J. Han, L. Wang, H. Dong and Y. Wang, *Chemical Engineering Journal*, 2022, **427**, 131808.

7 M. A. Yassin and A. A. M. Gad, *J Environ Chem Eng*, 2020, **8**, 104435.

8 X. Hao, Y. Liang, H. Zhen, X. Sun, X. Liu, M. Li, A. Shen and Y. Yang, *J Solid State Chem*, 2020, **287**, 121323.

9 S. Zhu, L. Zhao and B. Yan, *Microchemical Journal*, 2020, **155**, 104768.

10 X. Yang, M. Zhang, J. Xu, S. Wen, Y. Zhang and J. Zhang, *Spectrochim Acta A Mol Biomol Spectrosc*, DOI:10.1016/j.saa.2021.119553.

11 Y. Li, Y. Zhao, W. Zhang, K. Shao and H. Zhou, *Z Anorg Allg Chem*, 2021, **647**, 1091–1095.

12 M. Wang, P. Liu, H. Zhu, B. Liu and X. Niu, *Biosensors (Basel)*, DOI:10.3390/bios11080280.

13 M. Wang, H. Zhu, B. Liu, P. Hu, J. Pan and X. Niu, *ACS Appl Mater Interfaces*, 2022, **14**, 44762–44771.

14 S. Wei, Y. Yang, J. Li, J. Wang, J. Tang, N. Wang and Z. Li, *Chinese Chemical Letters*, 2023, 109114.

15 M. Liang, Y. Gao, X. Sun, R.-M. Kong, L. Xia and F. Qu, *J Hazard Mater*, 2024, **469**, 134021.

16 Y. Li, Y. Zhang, R. Javed, R. Li, H. Zhao, X. Liu, C. Zhang, H. Cao and D. Ye, *Food Chem*, 2024, **441**, 138315.